frontiers | Frontiers in Earth Science

TYPE Original Research
PUBLISHED 13 April 2023
DOI 10.3389/feart.2023.1169356

OPEN ACCESS

EDITED BY
Yunguo Li,
University of Science and Technology of China, China

REVIEWED BY
Kang Liu,
University of Science and Technology of China, China
Ema Frery,
Commonwealth Scientific and Industrial Research Organisation (CSIRO), Australia

*CORRESPONDENCE
Ugo Geymond,
geymond@ipgp.fr

SPECIALTY SECTION
This article was submitted to Geochemistry, a section of the journal Frontiers in Earth Science

RECEIVED 19 February 2023
ACCEPTED 30 March 2023
PUBLISHED 13 April 2023

CITATION
Geymond U, Briolet T, Combaudon V, Sissmann O, Martinez I, Duttine M and Moretti I (2023), Reassessing the role of magnetite during natural hydrogen generation.
Front. Earth Sci. 11:1169356.
doi: 10.3389/feart.2023.1169356

Reassessing the role of magnetite during natural hydrogen generation

Ugo Geymond[1,2]*, Théo Briolet[2,3], Valentine Combaudon[2,4], Olivier Sissmann[2], Isabelle Martinez[1], Mathieu Duttine[5] and Isabelle Moretti[4]

[1]Institut de physique du globe de Paris, CNRS, Université Paris Cité, Paris, France, [2]IFP Energies Nouvelles (IFPEN), Rueil-Malmaison, France, [3]Laboratoire de Géologie, Ecole Normale Supérieure, CNRS, PSL Research University, Paris, France, [4]Laboratoire des fluides complexes et de leurs réservoirs, CNRS, Université de Pau et des Pays de l'Adour, Pau, France, [5]Institut de chimie de la matière condensée de Bordeaux, CNRS, Université de Bordeaux, Pessac, France

Interactions between water and ferrous rocks are known to generate natural H_2 in oceanic and continental domains *via* the oxidation of iron. Such generation has been mainly investigated through the alteration of Fe^{2+}-silicate and some Fe^{2+}-carbonates. So far, magnetite (α-Fe_3O_4) has never been considered as a potential source mineral for natural H_2 since it is considered as a by-product of every known chemical reaction leading to the formation of H_2, despite it bears 1/3 of Fe^{2+} in its mineral lattice. This iron oxide is rather seen as a good catalyst for the formation of H_2. Recently, hydrogen emissions were observed in the surroundings of banded iron formations (BIF) that are constituted of, among other minerals, magnetite. Thus, this work is an attempt to constrain the true potential of magnetite by means of batch reactor experiments and additional thermodynamic calculations. It explores theoretical and experimental reaction pathways of magnetite during water-rock interactions, focusing on low temperatures (T < 200°C). For the purpose of the experiments, gold capsules filled with magnetite powders were run at 80°C and 200°C. Gas products were analyzed using gas chromatography (GC) while solid products were characterized by X-ray diffraction (XRD), Mössbauer spectroscopy, and scanning electron microscopy (SEM). After experimental alteration, high amounts of H_2 were quantified while mineralogical transitions were observed by SEM. It showed self-reorganization of the primary iron oxide resulting in sharp-edge and better crystalized secondary minerals. In parallel, XRD analyses showed tiny changes between the patterns of the initial powder and the solid products of reaction. Finally, Mössbauer spectroscopy revealed that the starting magnetite was partly converted to maghemite (γ-Fe_2O_3), a metastable Fe-oxide only containing Fe^{3+}. Major implications arise from these results. Concerning H_2 exploration, this work provides evidence that natural hydrogen can be generated at near-ambient temperature. It also infers that magnetite-rich lithologies such as BIF should be targeted while looking for H_2 source rocks. In addition, these outcomes could be of major interest for mining companies as they provide key elements to understand the formation of BIF-hosted iron ores.

KEYWORDS

natural hydrogen, magnetite, maghemite, water-rock interactions, mössbauer spectroscopy

1 Introduction

In the global context of the energy transition, exploration for natural H_2 is now starting especially in the continental domain (Larin et al., 2015; Gaucher, 2020; Boreham et al., 2021b; 2021a; Frery et al., 2021; Lefeuvre et al., 2021; Moretti et al., 2021). As such, understanding the physicochemical processes leading to its generation at depth is of prime interest. Among the mechanisms discussed in the literature, previous authors defined the following by order of decreasing estimated importance (Klein et al., 2020): 1) hydrothermal alteration and related iron oxidation, 2) radiolysis, 3) mechanoradicals, 4) volcanic degassing, and 5) biological production. Additional mechanisms, such as the late maturation of organic matter, should also be added to this list (Horsfield et al., 2022). The mechanism 1) corresponds to a redox reaction occurring in anoxic environments, where water oxidizes Fe^{2+} into Fe^{3+} and is reduced to form H_2. It can be summarized following the generic Eq. 1. Thus, targeting Fe^{2+}-rich lithologies for exploration is promising. In parallel, it is necessary to understand the behavior of such lithology while they interact with water. If H_2 generation through iron oxidation during water-rock interactions is now attested in the context of mafic and ultramafic rocks according to thermodynamic modeling as well as experimental and petrographic studies (Cannat, 1993; McCollom and Bach, 2009; Malvoisin et al., 2012), the potential of other Fe-rich lithologies remains poorly understood.

$$2Fe^{2+}O + H_2O \Leftrightarrow Fe_2^{3+}O_3 + H_2 \quad (1)$$

1.1 H_2 from Fe^{2+}-minerals alteration

Up to now, silicates have been by far the most extensively studied mineral family for sourcing H_2. Over recent decades, alteration of Fe^{2+}-bearing olivine and pyroxene by anoxic water has been frequently evidenced to generate H_2 during the serpentinization process at mid-oceanic ridges and later in continental domain (Cannat, 1993; Vacquand et al., 2018). The temperature strongly influences the kinetics of serpentinization and H_2 generation (McCollom, 2016) as well as the nature of the phases incorporating Fe during serpentinization (Tutolo et al., 2020). By-products of H_2 generation are magnetite (α-Fe_3O_4) at T > 200°C and Fe^{3+}-serpentine at T < 200°C (Eqs. 2, 3).

$$3Fe_2^{2+}SiO_4 + 2H_2O \Leftrightarrow 2Fe^{2+}Fe_2^{3+}O_4 + 3SiO_2 + 2H_2 \quad (2)$$

$$2(Mg,Fe^{2+})SiO_4 + 3H_2O \Leftrightarrow (Mg_2,Fe^{3+})(Fe^{3+},Si)O_5(OH)_4 + SiO_2 + H_2 \quad (3)$$

Lately, alteration experiments of Fe^{2+}-bearing amphibole (arfvedsonite) from peralkaline igneous intrusions were tested successfully to generate H_2 between 280°C and 400°C, associated with the growth of magnetite (Truche et al., 2021). In such settings where H_2-rich fluid inclusions were reported, aegirine was usually considered as the product of arfvedsonite alteration (Salvi and Williams-Jones, 1997; Potter et al., 2013) but was never observed during the experiments.

In addition to Fe-silicates, Fe-carbonates potentially sourcing H_2 were also investigated to a lower extent. In fact, H_2 emissions have been detected close to gold mineralization and banded iron formations (BIF) that are partly constituted by siderite ($FeCO_3$) and ankerite [(Fe,Ca)CO_3] (Boreham et al., 2021b; Geymond et al., 2022; Moretti et al., 2022; Malvoisin and Brunet, 2023). Associated thermodynamic calculations at T < 200°C showed that siderite could be the source of such emissions (Malvoisin and Brunet, 2023), which remains to be confirmed by further studies. Another experimental study demonstrated that siderite is destabilized in contact with water to form secondary magnetite at T > 300°C, with associated H_2 found in the free gas phase (Milesi et al., 2015). The process can be summarized by Eq. 4.

$$3Fe^{2+}CO_3 + H_2O \Leftrightarrow Fe^{2+}Fe_2^{3+}O_4 + H_2 + 3CO_2 \quad (4)$$

1.2 Current knowledge of H_2 formation involving magnetite

Despite a remnant of Fe^{2+} in its chemical formula, magnetite has never been considered as a potential source for natural H_2 since it is usually viewed as a by-product of every redox reaction involving Fe-rich phase and hydrogen generation (see Eqs. 2–4). On the contrary, it has been suggested that magnetite may act as a catalyst during H_2 generation related to Fe oxidation (Neubeck et al., 2011; Mayhew et al., 2013) or during the conversion of CO_2 into abiotic CH_4 during the Sabatier's reaction (Eq. 5) as discussed in the literature in contexts where H_2 is naturally generated (Etiope, 2017; Etiope et al., 2017). Such a catalytic effect is even extended to the whole spinel group minerals like chromite ($FeCr_2O_4$) and could originate at the spinel surfaces where electron exchanges are enhanced due to the singular mineral structure (Mayhew et al., 2013).

$$CO_2 + 4H_2 \Leftrightarrow CH_4 + 2H_2O \quad (5)$$

The present work is an attempt to assess the potential of magnetite to generate H_2 from the oxidation of its remnant Fe^{2+}, based on batch experiments and thermodynamic modeling. It particularly focuses on the case of BIF since H_2 emissions have been observed in their vicinity and magnetite is a major component of these formations.

2 Banded iron formations and H_2 generation

BIF are sedimentary rocks of marine origin and Precambrian age and hold as a consequence important clues to understand primitive Earth and the appearance of life. They also stand as a major reservoir of iron, exploited worldwide. As such, their dynamics of formation and evolution through the ages have been a matter of numerous studies for a long time, notably since they are highly exploited by mining companies (Ramanaidou and Wells, 2014). Recently, BIF were suggested as a potential new lithology able to source H_2 in continental domain (Moretti et al., 2021). In fact, their presence in the subsurface was attested below H_2 seepages for instance in Namibia and Brazil. Additional suspected seepages have also been reported in the surroundings of BIF-hosted iron mines in Australia and South Africa (Geymond et al., 2022; Moretti et al., 2022). In addition to the spatial correlation between BIF and H_2 emissions, BIF carry key Fe-minerals that are promising for H_2 generation and need to be tested experimentally and thermodynamically. BIF correspond to alternate

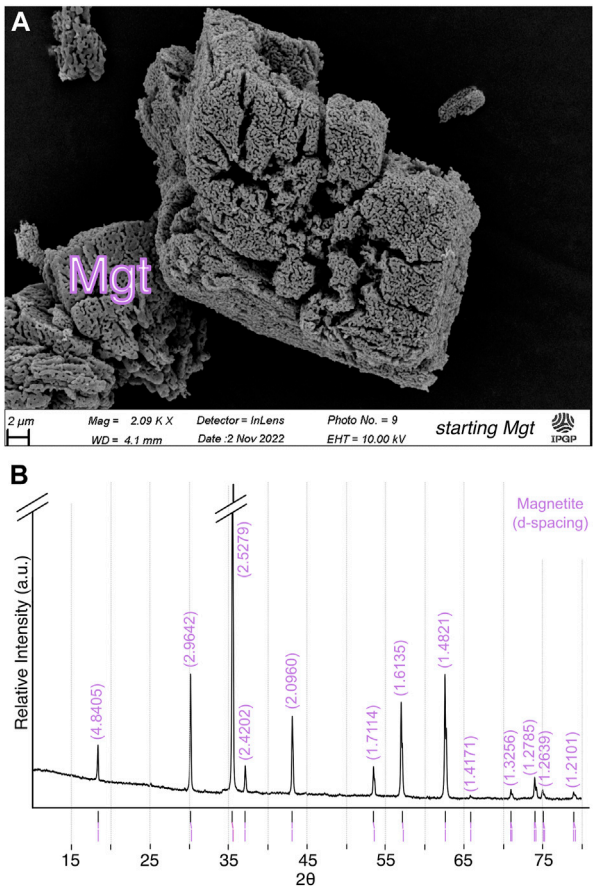

FIGURE 1
(A) SEM image and **(B)** XRD analysis of the starting magnetite. Mgt refers to magnetite. Please note the narrowness and the highness of the diffraction peaks that highlight the quality of the crystallinity. A zoomed image of the starting magnetite surface is provided in Figure 3.

layers of iron oxides and iron silicates or carbonates in a quartz matrix. Such formation can reach several hundreds of meters in thickness. While BIF are preserved from surficial alteration, primary Fe-oxides are usually magnetite or hematite. Fe-silicates are diverse and consist mainly of stilpnomelane, riebeckite, or minnesotaite. Finally, Fe-carbonates are usually siderite or ankerite. Marginal sulfurs like pyrite are also found (Klein, 2005). In BIF, Fe speciation ranges from essentially Fe^{2+} at depth to almost exclusively Fe^{3+} toward the surface. This supergene oxidation leads to the formation of iron ores and is related to the leaching of the rock by meteoric water in equilibrium with atmospheric oxygen. Since they are very stable in oxidative environments, goethite (FeO(OH)) and hematite (α-Fe_2O_3) are the main minerals found at the surface where BIF are weathered (Cornell and Schwertmann, 2003). Sometimes, maghemite (γ-Fe_2O_3) is present as well, corresponding to a transitionary state from primary magnetite to secondary hematite. At depth, authors have described some oxidized horizons far from the surface and associated with the alteration of primary minerals during hypogene processes and replacement by secondary iron oxides (Angerer et al., 2015; Duuring et al., 2019). This alteration likely originates from the circulation of anoxic groundwater. Constraining through experiments and thermodynamic modeling the generation of H_2 during BIF weathering when anoxic water circulates at depth is key to determine the real H_2 potential of this lithology.

3 Batch reactor set up

3.1 Starting material and protocol

Batch reactor experiments were performed on magnetite using a chemically synthetized powder produced by Sigma-Aldrich. As shown in Figure 1A, the magnetite powder consisted in grains of ±10 µm with a very high microporosity and sub-grains of typically 200 nm, providing a high reactive surface (2.0 ±0.1 m^2/g according to BET analyses) and thus favoring high reaction kinetics. The mineral powder was characterized prior to the experiments in order to ensure mineral quality. Figure 1B confirms the purity of the sample through *X*-ray diffraction analysis. Rock-Eval analyses (step-heated pyrolysis and combustion) were also conducted to determine total organic content (TOC) at 0.01 wt%, highlighting no organic matter was trapped in the mineral lattice. It must be noted however that this value falls within the Rock-Eval detection limit, also at 0.01 wt%.

Gold capsules of 1 mL were cleaned by means of a nitric acid bath before being heated in an oven at 650°C for 1 h. To ensure anoxic conditions, they were then filled under nitrogen atmosphere with ±200 mg of magnetite and ±400 mg of Milli-Q water at 18.2 MΩ in order to obtain water-rock mass ratios of 2 for all capsules. It should be noted that the water was previously degassed to remove all dissolved O_2, which could have acted as the primary oxidizing agent of Fe^{2+} of the starting powder during the experiment instead of H_2O. The capsules were sealed and a first set was run in a reactor at 200°C/200bar for 2 months. To explore H_2 generation in a large range of P/T conditions, a second set of duplicates was launched at 80°C/100bar. To compensate for the presumably less favorable H_2 generation kinetics at this lower temperature, an extended duration of 4 months was chosen for this set of experiments. Capsules only containing water were also run at the same time for both sets of experiment as blanks to quantify any bias potentially introduced by the experimental protocol. To verify the reproducibility of the results, each series of experiments was conducted twice. Table 1 summarizes the initial parameters for each capsule.

3.2 Analytical techniques

The experiments were stopped by rapidly quenching the batch reactor to ambient temperature. The capsules were pierced and the gas phases were extracted under vacuum in gas-tight glass containers. Gas products were analyzed by gas chromatography (GC) using a GC-BID 2030 from Shimadzu equipped with a Restek RT-Q-BOND 30 m × 530 mmID column. H_2 and CH_4 were quantified by using a dedicated method implemented for this purpose. After the calibration, ±14% (H_2) and ±8% (CH_4) uncertainties were determined by calculating standard deviation from gas standards. O_2+Ar, N_2 and CO_2 were also detected but not quantified. Solid products were recovered and analyzed by scanning electron microscopy (SEM), *X*-ray diffraction (XRD), and Mössbauer spectroscopy in order to study the reactions that occurred during magnetite alteration. SEM sessions were

TABLE 1 Summary of experimental settings for each capsule. Mgt refers to magnetite.

	React	Pow (mg)	Water (mg)	W/R ratio	T (°C)	P (bar)	t (month)
M200_1	Mgt	191.3	400	2.09	200	200	2
M200_2	Mgt	190.8	400	2.10	200	200	2
Blank200			400		200	200	2
M80_1	Mgt	185.9	400	2.15	80	100	4
M80_2	Mgt	192.6	400	2.08	80	100	4
Blank80			400		80	100	4

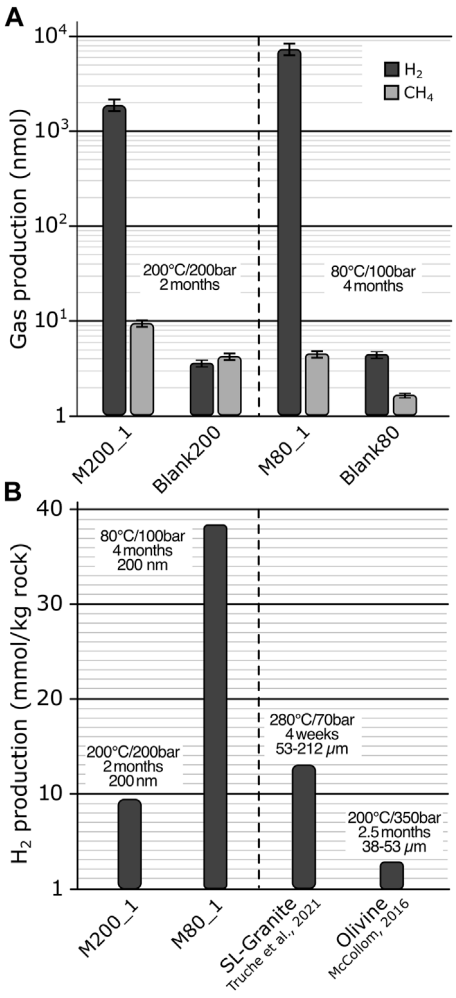

FIGURE 2
(A) H_2 and CH_4 generation from magnetite and blank capsules, obtained after gas chromatography and expressed in nmol. Uncertainties are given in percentage of the measurements, ±14% for H_2 and ±8% for CH_4. **(B)** Results are compared to similar experiments on olivine (McCollom, 2016) and ferrous granite from Strange Lake, Canada (Truche et al., 2021).

performed on a Zeiss Auriga 40 (IPGP, Paris) equipped with a 1 nm resolution FEG and a Quantax 800 EDS feature with a XFlash 410-M detector. XRD measurements were done on an Empyrean diffractometer (@Malvern-Panalytical) equipped with a copper tube (Kα = 1.541874 Å) and a multi-channel PIXcel detector (UPC, Paris). The chosen angular range was between 5° and 80°, the step size was 0.007°, and the time per step was 80 s (i.e., 1 h measurement per sample). For ^{57}Fe Mössbauer spectroscopy, each powder was analyzed with a constant acceleration Halder-type spectrometer (ICMCB, Bordeaux) equipped with a ^{57}Co radioactive source (embedded in a Rh matrix), which was maintained at 293 K. The spectrometer was calibrated using a pure α-Fe^0 foil as an external reference. All spectra were recorded in transmission geometry at ambient temperature. The Mössbauer hyperfine parameters and the relative areas of each component were refined with the WinNormos software (Wissenschaftliche Elektronik GmbH). Each analysis lasted about 1 day. The results initially provided in % of the peak area could be expressed in at% in a thin-absorber approximation (Kuzmann et al., 2003). The given uncertainty was 3 at%.

3.3 Thermodynamic modeling

In order to interpret our experimental results, thermodynamic equilibrium was studied for magnetite alteration reactions in the same batch configuration. PhreeqC and PhreePlot computer codes developed by the US Geological Survey were used, together with the thermodynamic database "Thermodem" developed by the BRGM. This database was selected because of its very complete dataset for Fe-oxides. Calculations were done in a closed system, respecting a water-rock ratio of 2 as in the experiments: 200 mg of mineral and 400 mg of pure water. The modeling was conducted between 25°C and 225°C. Since our calculations demonstrated no major impact of pressure conditions, the results presented in this paper are given for a constant pressure of 200 bar. As noticed by previous authors, no headspace remained in gold capsules during experiments due to the elevated pressure (Milesi et al., 2015). Thus, no headspace allowing the free gas phase to form by gas exsolution from water was considered for our numerical modeling, but only dissolved species.

4 Experimental results

4.1 Gas products

GC results for the experiments and associated blanks at 80°C and 200°C are provided in Figure 2A. All measured gases were dissolved

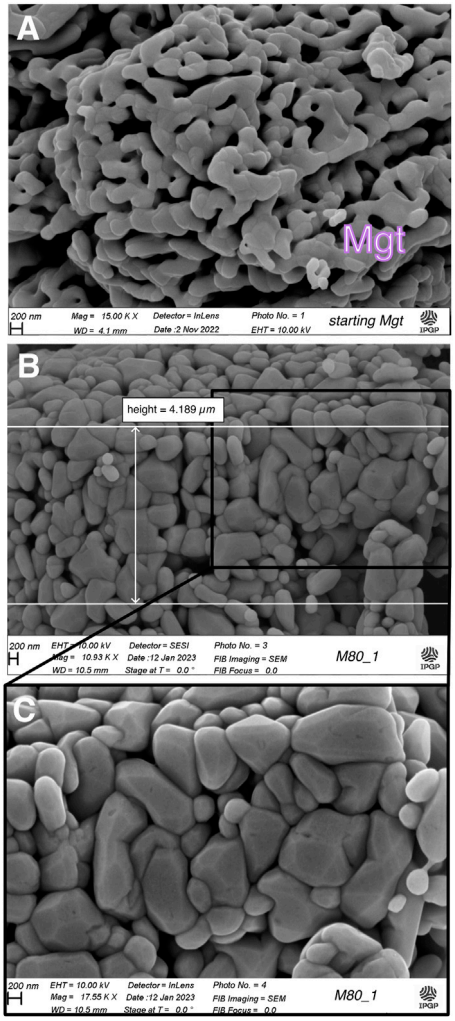

FIGURE 3
SEM images of **(A)** the starting magnetite compared to **(B)** magnetite after alteration at 80°C from M80_1 capsule. Note the higher mineral density and better crystallization after alteration. Mgt refers to magnetite. **(C)** Zoom of an altered magnetite surface from **(B)**, highlighting mineral sharp edges.

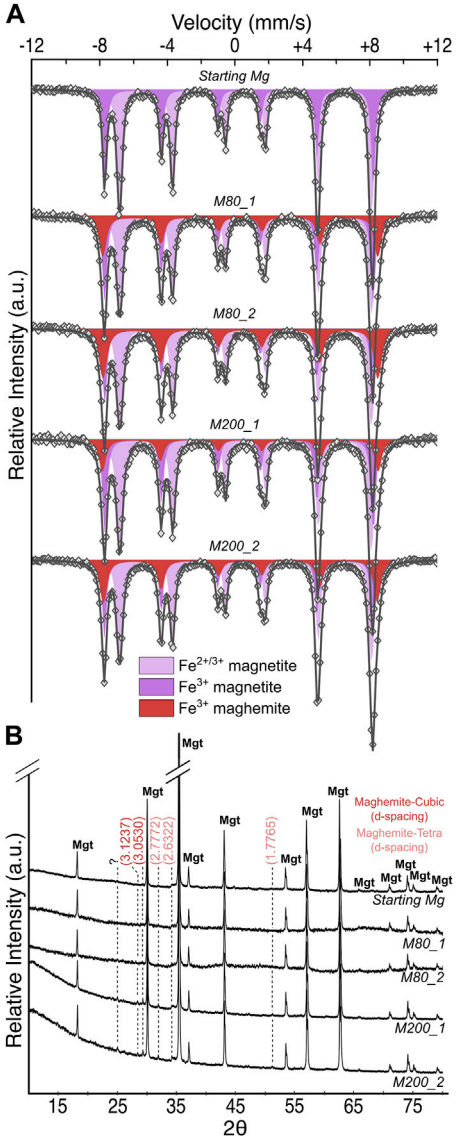

FIGURE 4
(A) Room temperature Mössbauer spectrum for starting magnetite and solid products from M200_1, M200_2, M80_1, and M80_2. For quantitative results, see Table 2. **(B)** XRD results for the same powders. Mgt refers to the peaks previously correlated to magnetite (see Figure 1). Note the appearance of new peaks for altered powders that can be attributed to maghemite in both tetragonal and cubic crystal systems.

during experiments since no free headspace was left in the gold capsules due to the elevated pressures. For blank experiments, no significant amount of CH_4 or H_2 was quantified (4.57 nmol H_2 and 1.66 nmol CH_4 for Blank80, 3.64 nmol H_2 and 4.29 nmol CH_4 for Blank200), suggesting that the methodology presents no major bias. Gas collected after magnetite alteration contained significant amounts of H_2, even more at 80°C (7.10 µmol) than at 200°C (1.8 µmol). From these magnetite capsules, very low amounts of CH_4 were also quantified at 80°C and 200°C with 4.7 nmol and 9.9 nmol, respectively. These amounts of methane, just above the CH_4 levels for blank capsules, are likely to originate either from the cracking of traces of organic matter present in the starting magnetite or from organic contaminations during capsules filling. In Figure 2B, results are expressed in mmol/kg rock in order to be compared with previous experiments conducted on olivine grains (38–53 µm) at 200°C for 2.5 months and grains of Fe-rich granite from Strange Lake (53–212 µm) at 280°C for 1 month (McCollom, 2016; Truche et al., 2021). These experiments have been selected for comparison with our runs due to the similarities in terms of methodology (experiments on rock/mineral powder, alteration in gold containers). H_2 generation from our highly porous magnetite is in the same order of magnitude as observed from other minerals. Indeed, the magnetite tested at 200°C/200bar generated around 10 mmol/kg rock, which falls between the production of peralkaline granite and olivine 13 mmol/kg rock and 2.9 mmol/kg rock, respectively. The magnetite tested at 80°C/100bar generated close to 38 mmol/kg rock, corresponding to almost fourfold the amount of H_2 produced at 200°C/200bar. It must be kept in mind,

TABLE 2 Quantitative results of room temperature Mössbauer analyses for both duplicate experiments at 80°C and 200°C, expressed in at%. The uncertainty is 3 at%. For related Mössbauer spectra, see Figure 4. For related hyperfine parameters, see Supplementary Table S1.

	magnetite		maghemite
	$Fe^{2+/3+}$ octa	Fe^{3+} tetra	Fe^{3+}
Starting Mgt	62 (3)	38 (3)	
M80_1	51 (3)	32 (3)	17 (3)
M80_2	48 (3)	26 (3)	26 (3)
M200_1	47 (3)	31 (3)	22 (3)
M200_2	44 (3)	25 (3)	31 (3)

however, that direct comparison of one experiment to another remains biased, since starting parameters, such as reactive surface, duration, or temperature, differ.

4.2 Solid products

4.2.1 SEM observations

SEM observations are presented in Figure 3. The initial magnetite consists of sub-grains of ±200 nm in size bonded together, as visible in Figure 3A. On the opposite, the powder after alteration show a clear self-reorganization of the initial grains (Figure 3B). In fact, grains after alteration exhibit very cohesive and better-shaped minerals that filled the initial porosity. Figure 3C highlights sharp edges of the new minerals, which contrasts with the starting material. Such a pattern is observed for every solid product of reaction, at both 80°C and 200°C. Since the surfaces of the starting magnetite are not visible anymore after reaction, the exact mineralogical transitions that occurred during alteration cannot be pointed out unambiguously by SEM observations.

4.2.2 Mössbauer and XRD analyses

Mössbauer spectroscopy and XRD results giving access to both Fe speciation and related Fe-bearing mineralogy are presented in Figure 4A. Mössbauer analyses show pure magnetite for the starting powder. In contrast, all run products from both the 80°C and 200°C experiments exhibit newly formed maghemite (γ-Fe_2O_3) in addition to the remaining initial magnetite. Past studies demonstrated the ease to differentiate maghemite from magnetite using Mössbauer analyses at room temperature (Joos et al., 2016), and the solidity of the spectra interpretation. Quantitative results provided in Table 2 show a high dispersion in Fe_{Mgh}/Fe_{tot} ratios for duplicates at both temperatures: 17% ±3% (M80_1) and 26% ±3% (M80_2) at 80°C, 22% ±3% (M200_1) and 31% ±3% (M200_2) at 200°C. This could be explained by the difficulty to perfectly reproduce the same experimental conditions for each capsule, as well as the given uncertainty of the Mössbauer method (±3 at%). However, the maghemite contents are globally lower for the experiments at 80°C than at 200°C. In terms of crystallography, maghemite can be described as a magnetite where all Fe^{2+} has been oxidized to Fe^{3+}. The gain of charge is compensated by punctual cation vacancies in the mineral lattice. In the literature, maghemite is observed as cubic spinel

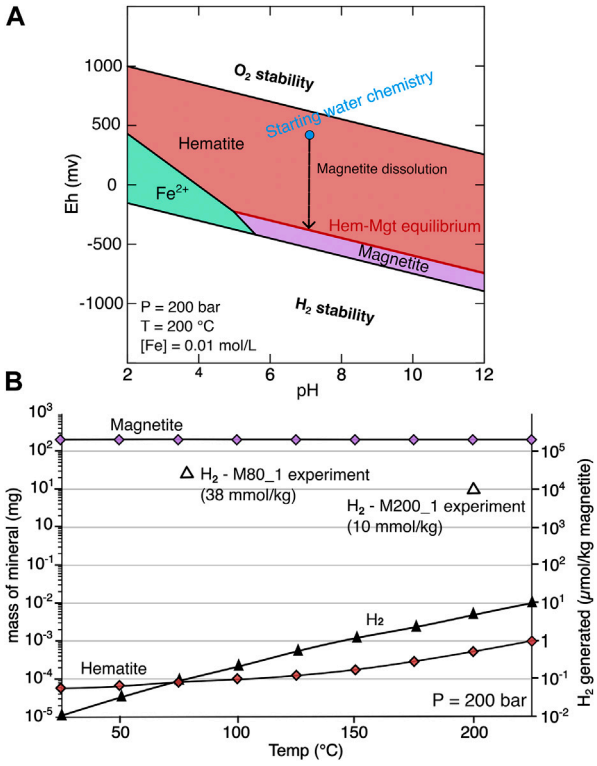

FIGURE 5
(A) Stability of Fe-oxides at 200°C/200bar, seen in an Eh-Ph diagram. Starting conditions for the modeling is plotted in blue and falls in the hematite domain. Hem refers to hematite, Mgt refers to magnetite. **(B)** Thermodynamic equilibrium after magnetite alteration for a water-rock ratio of 2, between 25°C and 225°C. Please note that the Y-axes for mineral mass and H_2 generated are in log-scale.

crystals just like magnetite while the vacancies are distributed randomly or observed as tetragonal spinel crystals while vacancies have a higher degree of ordering (Grau-Crespo et al., 2010). Due to these similar crystallographic properties, differentiating maghemite from magnetite using XRD analyses is difficult (Winsett et al., 2019). However, XRD patterns of our alteration products are compared with the starting magnetite in Figure 4B. Thanks to careful peak indexing of the starting magnetite (see Figure 1A), new peaks slightly visible on alteration products diffractograms can be identified. All these peaks, except one around 2θ = 25, match with maghemite, giving more credit to Mössbauer analyses. Part of these new peaks match the maghemite tetragonal structure, while others rather match the cubic structure. In addition, it is worth pointing out that new maghemite peaks are bigger for both duplicates at 200°C than at 80°C. This could be explained by amorphous maghemite being barely detected at 80°C versus better crystalized maghemite detected at 200°C, since XRD only detects well-crystalized phases. However, Mössbauer analyses, that detects amorphous and crystalized phases with the same precision, revealed more maghemite formed in the run products for higher temperature experiments, providing a simple explanation for the bigger peaks observed on XRD patterns of 200°C experiments.

5 Discussion

5.1 Observed vs. theoretical magnetite reactivities from experimental and numerical modeling

In order to widen the discussion, numerical modeling was conducted in addition to experiments. Before launching further calculations, the stability of magnetite regarding our experimental settings was estimated by constructing Eh-pH diagrams of iron between 25°C and 225°C. Since all the Eh-pH diagrams were comparable to each other, only the one at 200°C/200bar is discussed and provided in Figure 5A. It shows that, in the domain of water stability, iron is partitioned into three phases at the thermodynamic equilibrium. The most acidic and reducing conditions ensure Fe speciation remains aqueous as Fe^{2+}. Elsewhere in the diagram, Fe precipitation is favoured either as magnetite when conditions are very reducing or as hematite when conditions are more oxidizing. Since water-rock reactions involving H_2 generation only occur in anoxia —otherwise O_2 acts as the oxidizing species towards iron oxidant while H_2O is not reduced— a pure water was used for our calculations (Eh = ±300 and pH = ±7). It is interesting to see on the Eh-pH diagram that the H_2O falls in the stability domain of hematite. Then, regardless of kinetics or activation energy barriers, magnetite seems thermodynamically able to destabilize upon contact with anoxic water to form hematite and H_2 related to a higher degree of Fe oxidation. This observation confirms the experimental results that showed the destabilization of magnetite at both 80°C and 200°C. However, it is interesting to point that maghemite was formed during our experiments rather than hematite as predicted by the Eh-pH diagrams. To our mind, the presence of maghemite in our experiments reflects a transitionary state where thermodynamic equilibrium was not reached, while the numerical modeling reflects the steady state equilibrium without any consideration for kinetics. In fact, laboratory experiments may not always reach equilibrium, which is a known limitation of analog modeling of fluid-rock interactions. It originates from the relatively short duration of experiments that last weeks or months compared to the long periods of time involved to reach thermodynamic equilibrium of reactions at geological timescales. In addition, ideal synthetic material for experiments such our nanometric and highly porous magnetite are not found in nature. Such discrepancies should be kept in mind while extrapolating experimental results to natural environments.

Then, magnetite alteration in anoxic water was tested numerically using the same conditions as the experiments, namely, 200 mg of pure magnetite reacting with 400 mg of pure degassed water in a closed reactor with no headspace. Thermodynamic equilibria of reactions are presented in Figure 5B. Surprisingly, the magnetite appears very stable, with almost all the initial powder unaltered (200 mg) regardless of the temperature. Consequently, the modeling shows very small amounts of precipitated hematite, inferior to magnetite amounts by five to six orders of magnitude depending on the temperature. The numerical generation of H_2 follows the same trend as the hematite formation and thus remains very low in the whole set of temperature ranging only from 2 to 10 µmol/kg mineral. This generation is far from the measured generation from our experiments (as high as 40 mmol/kg mineral at 80°C) or the generation of few mmol/kg olivine estimated by previous thermodynamic calculations (McCollom and Bach, 2009). Even if the numerical modeling shows that magnetite is not fully stable in the chosen conditions, it appears poorly reactive despite the starting conditions falling in the domain of hematite stability. This cannot be explained by an activation energy barrier since some hematite succeeds to form in the whole range of temperatures during the calculations. To our mind, the lack of magnetite converted into hematite in our numerical modeling rather originates in a strong change of the redox conditions for minor amounts of magnetite destabilized, particularly since the water-rock ratio is low. In fact, the initiated dissolution of magnetite dramatically reduces the environment, until reaching new conditions where the low amounts of hematite formed and the initial magnetite can co-exist, as schematized in Figure 5A. On the contrary, our experiments conducted at 80°C and 200°C showed the formation of significant quantities of maghemite in all solid products, with Fe_{Mgh}/Fe_{tot} ranging between 17 and 33 at% at the end of the runs. The conversion from magnetite to maghemite was validated by maghemite peaks in the XRD patterns (essentially visible at 200°C) as well as SEM observations that highlighted a strong reactivity of magnetite during experiments. Such experimental results contrast with the thermodynamic simulations as they depict very different magnetite behaviors in the same context. In order to numerically model the exact system that we observed during our experiments and offset kinetic effects, it must be noted that the calculations were also conducted by inhibiting the precipitation of all Fe-oxides except magnetite and maghemite, however magnetite never showed a greater reactivity. Thus, we interpret the discrepancies in magnetite alteration rates between thermodynamic calculations and experiments as the result of currently approximate thermodynamic constants for metastable Fe-oxides such as maghemite. These are hard to constrain, but should probably now be re-evaluated. Such a discrepancy between thermodynamics and observations while studying maghemite has already been mentioned in the past. Up to now, it was suggested that it could originate in the singular structure of maghemite hosting vacancies that are filled by H^+ and are not easily accounted for by thermodynamic modeling (Elder, 1965).

5.2 Magnetite alteration in anoxic conditions: A new source for H_2 generation

At T < 225°C, the simulations suggested that magnetite has a low potential for H_2 generation in anoxia regarding its theoretical high stability. In fact, in the tested conditions, no more than a few µmol/kg magnetite of H_2 was estimated to form associated with the oxidation of some Fe^{2+}, with a maximum of 10 µmol/kg magnetite at 225°C. On the contrary, high amounts of H_2 were measured during the experiments with 38 mmol/kg magnetite and 10 mmol/kg magnetite at 80°C and 200°C, respectively. This generation was observed concomitant with the formation of new maghemite coupled with magnetite destabilization and oxidation of Fe^{2+}. Up to now, the conversion of magnetite into maghemite had always been evidenced experimentally in oxic conditions (Elder, 1965; Swaddle and Oltmann, 1980), which can be summarized by

Eq. 6. The present work demonstrates that an additional mechanism can lead to the formation of maghemite from magnetite destabilization, where water is the oxidizing agent and is reduced to form H_2. Thus, we suggest Eq. 7 as a new chemical reaction to describe the generation of H_2 during magnetite alteration at T < 200°C.

$$2(\alpha - Fe_3O_4) + \frac{1}{2}O_2 \Leftrightarrow 3(\gamma - Fe_2O_3) \quad (6)$$

$$2(\alpha - Fe_3O_4) + H_2O \Leftrightarrow 3(\gamma - Fe_2O_3) + H_2 \quad (7)$$

Concerning the amounts of H_2 generated during the experiments and the reaction yields, it is tempting to extrapolate the Mössbauer results based on Eq. 7 and compare them to the gas results to check the consistency between both gaseous and solid products of reaction. Nonetheless, magnetite crystals are commonly non-stochiometric in their octahedral sites, meaning that the amounts of Fe^{2+} in magnetite cannot be simply estimated as half the amount of $Fe^{2+/3+}$ octa. (Daniels and Rosencwaig, 1969). Therefore, our Mössbauer results do not provide the means to determine the exact initial budget of Fe^{2+} in the starting magnetite, as well as the remaining Fe^{2+} budget in the altered magnetites of the run products. It is thus not reasonable to estimate H_2 production from Fe^{2+} that was oxidized during weathering. XRD and Mössbauer analyses suggested, however, a higher rate of magnetite conversion into maghemite at 200°C than at 80°C, which should have been positively correlated with higher levels of H_2 at 200°C than at 80°C following Eq. 7. On the contrary, the opposite trend has been observed. Some factors can already be disqualified to explain this opposite trend. Firstly, variations of reactive surface largely influencing reaction kinetics from one experiment to another is possible (even though unlikely since the same initial powder was used for each experiment) but a positive correlation between maghemite formed and H_2 generated would have been observed anyway. Secondly, many redox reactions leading to H_2 generation like serpentinization are known to require the solubilization of Fe^{2+} from the starting mineral altered (olivine) before iron oxidation and incorporation into the secondary mineral (magnetite). Knowing the dissolved Fe^{2+} and Fe^{3+} concentrations in the aqueous phase as well as the rates of formation of the secondary mineral are helpful to constrain the whole system. Iron could have oxidized and generated H_2 without precipitating secondary minerals yet due to lowered kinetics of precipitation at low temperature. In the case of magnetite alteration into maghemite, however, Fe oxidation occurs *in situ* in the mineral lattice, without any Fe solubilization. Thus, neither the variability in Fe concentration in the aqueous phase nor the variability in the maghemite formation rates between 80°C and 200°C experiments can explain the opposite trend observed. We suggest this apparent discrepancy between H_2 and maghemite formation could rather originate from:

(i) A poor quantification of H_2 quantities during capsule piercing and later GC analyses. Duplicates of gas measurements would have helped assessing this point but were not realized in this study;
(ii) A poor Mössbauer quantification of maghemite amounts formed during the experiments. In order to refine maghemite quantification, the use of other relevant analytical tools, able to distinguish magnetite and maghemite as well as to quantify them, should be performed simultaneously with Mössbauer spectroscopy. For instance, previous works demonstrated that maghemite is easily differentiated from magnetite by Raman spectroscopy (Hanesch, 2009), while magnetic studies allow their quantification (Nazarova et al., 2000);
(iii) O_2 contamination during the filling of the capsules that consumed part of the H_2 generated at 200°C;
(iv) O_2 contamination during the filling of the capsules that artificially led to the formation of maghemite without generating any H_2 at 200°C, following Eq. 6;
(v) A still imperfect comprehension of how maghemite forms and evolves from magnetite to form H_2. For instance, it has been suggested that H^+ enters the vacancies of maghemite to stabilize the spinel structure (Elder, 1965; Swaddle and Oltmann, 1980). Thus, a partial consumption of H_2 during maghemite formation should not be disregarded.

5.3 Extrapolation to natural environments

Batch reactor experiments coupled with numerical modeling were performed since these approaches have long been used to study H_2 generation in natural environments, particularly during serpentinization (McCollom and Bach, 2009; Malvoisin et al., 2012; Crouzet et al., 2017). They allow the understanding of water-rock interactions and related chemical processes at a fundamental scale by working in fully-controlled systems and covering a wide range of physical and chemical parameters such as temperature, pressure, or f_{O_2}. However, the methodology presents some limitations that need to be considered before extrapolating results to natural environments. Closed systems, where parameters are ideally controlled, attempt to mimic natural opened environments that are much more complex in every way. Mineral powders are not equivalent to cohesive rocks in terms of porosity or surface reactivity. Finite volumes of initial pure water rapidly reaching an equilibrium state in batch systems are not equivalent to water flow in aquifers where water is always regenerated and never equilibrated with surrounding rocks like in many natural systems. In addition, even with the same starting parameters, water-rock interactions could slightly differ from one experiment to another in terms of reaction kinetics and yield due to different capsule volumes and tiny heterogeneities in powders such as aggregated grains. Then, our results should be extrapolated to natural environments cautiously, and in terms of qualitative mechanisms leading to H_2 generation rather than quantitative volumes of generated gas. This study, even if it does not provide precise quantification or constraints about kinetics, reveals a new mechanism for H_2 generation originating from the alteration of magnetite in anoxic environments. In our opinion, this discovery holds significant implications for understanding natural hydrogen systems.

5.3.1 Enrichment and oxidation of iron in BIF and related H_2 generation potential

Since magnetite is a very common mineral in Earth's crust, these new insights widen the number of potential source rocks to focus on while looking for natural hydrogen generation or accumulations. Therefore, the potential of BIF needs to be further investigated. More precisely, the H_2 potential of Archean to Mesoproterozoic BIF is high and should be targeted as a priority as they carry thick layers of almost pure magnetite, as visible in Figure 6. For instance, the BIF from the Quadrilatero Ferrifero in the Sao Francisco Basin in Brazil and

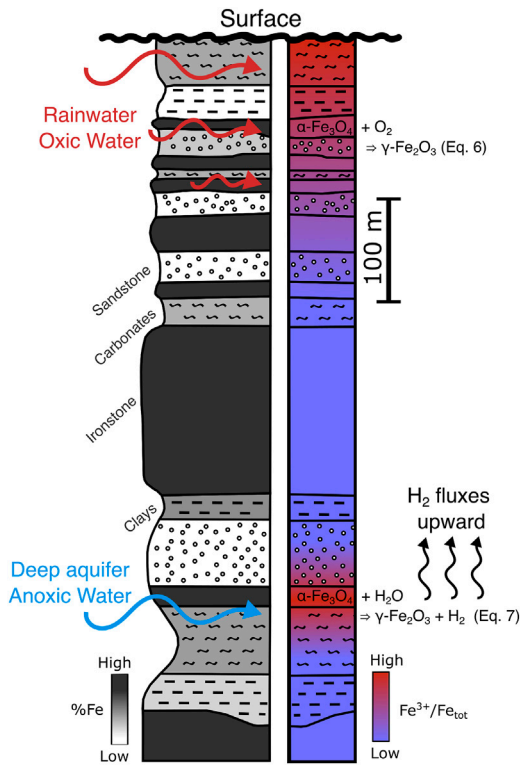

FIGURE 6
Schematic view of a late Archean BIF from Hamersley (Australia) and the related mineralogy, iron content, and iron speciation depending on the depth. In BIF, maghemite (γ-Fe_2O_3) grows during magnetite (α-Fe_3O_4) alteration by oxic water at the surface. We propose here a second process at depth: The alteration of magnetite by anoxic water that leads to the generation of H_2.

the Western Australian Yilgarn craton belong to this period. On the contrary, the H_2 potential of Neoproterozoic BIF seems lower as their Fe-oxide rich layers are rather constituted by hematite levels (Klein, 2005), even if they also carry Fe-minerals of interest like siderite. In the case of Archean to Mesoproterozoic BIF, it is interesting to note that this study provides evidence that establishes a correlation between H_2 seeps suspected at the surface and iron enrichment and oxidation described in the subsurface. In fact, the presence of magnetite altered into maghemite has been largely investigated for the last decades as it furnishes clues to understand the formation of BIF-hosted iron ores. This mineralogical transition is well documented in shallow as well as deeper ironstone layers (Morris and Ramanaidou, 2007; Ramanaidou and Wells, 2014). Close to the surface, the transition is commonly attributed to the circulation of oxygenated water that leaches BIF, as presented in Figure 6. On the contrary, the presence of maghemite at depth could be concomitant with H_2 generation while anoxic water circulates, as already suggested (Geymond et al., 2022).

5.3.2 H_2 generation during serpentinization

During serpentinization, magnetite has long been considered as the by-product of H_2 generation. This work, however, shows that magnetite can be altered in aqueous media to form maghemite, triggered by the oxidation of iron to higher grades. Due to their similarities, maghemite and magnetite are hardly differentiated by conventional mineralogical characterization methods like XRD, raising several questions:

(i) Is the Fe-oxide formed during serpentinization rather magnetite or maghemite?
(ii) If magnetite is the Fe-oxide formed during the primitive stages of serpentinization, can it oxidize into maghemite during subsequent episodes of serpentinization or alteration?

Previous studies based on remanence and magnetic susceptibility analyses on serpentinized rocks confirmed that maghemite is commonly found in such samples in addition or in replacement to magnetite (Saad, 1969; Nazarova, 1994; Nazarova et al., 2000). Answering such questions could necessitate the reassessment of Fe-oxidation yields during serpentinization, and consequently the quantities of H_2 generated in the process.

5.3.3 Pressure-Temperature domains for H_2 generation in cratonic areas

Since the discovery of H_2 vents at mid-oceanic ridges, extensive studies have been conducted to determine optimum Pressure-Temperature conditions in order to generate H_2 from serpentinization. Numerical and experimental modeling established the optimum temperature for H_2 generation of around 300°C with a limited impact of pressure, at least for serpentinization (McCollom and Bach, 2009; Klein et al., 2013). In this context, a high heat supply, mainly provided by the cooling of the upwelling mantle right below the spreading center (Allen and Seyfried, 2004), creates a geothermal gradient that ranges from 40°C to 80°C/km. In contrast, the geothermal gradient in continental crust is usually lower since the lithosphere is thicker. In Precambrian shields, especially where many H_2 emissions are detected, the modern geothermal gradient is approximately 20°C–25°C/km (Barbier, 2002). Thus, the range of temperatures required to form H_2 in continental domain is now being questioned, since elevated temperatures would require very deep water-rock interactions. Evaluating the range of temperature and kinetics required to form H_2 are key points to determine the "sustainability" of the natural hydrogen resource. Up to now, only few studies focusing on olivine alteration demonstrated experimentally that H_2 can be generated at near-ambient temperature (Neubeck et al., 2011). Subsequently in natural environments, it is still unclear whether the H_2 emissions result in 1) a past generation during water-rock interactions at high temperature where H_2 was trapped and stored until today or 2) a present and continuous generation during water-rock interactions at lower temperatures. Fluid inclusions hosting H_2 found in some cratonic rocks (Truche et al., 2021) would point toward point 1). In the present paper, we experimentally showed that H_2 forms at 80°C (in addition to 200°C), giving credit to point 2) with a possible generation at near-ambient temperature in natural environments. Consequently, water-rock interactions could source H_2 at present-day in low-temperature geosettings. Such results could explain why no fall of pressure is remarked in the hydrogen reservoir exploited in Mali, if we make the assumption of a continuous refill during exploitation by a current generation at depth (Prinzhofer et al., 2018).

6 Conclusion

Up to now, magnetite (α-Fe_3O_4) was only considered as a catalyst for H_2 generation despite the fact its total iron content bears a remnant of Fe^{2+} (one-third, theoretically). This belief could originate from the observation of magnetite as a product of redox reaction involving Fe oxidation and H_2 generation, in natural environments as well as in laboratory experiments and numerical modeling. As it is one of the main rock-forming minerals in banded iron formations (BIF) in the vicinity of which H_2 emissions have been detected, the present work aimed to qualitatively assess the real potential of magnetite to source H_2 during water-rock interactions by conducting batch reactor experiments and thermodynamic calculations. The results of our experimental study demonstrated that magnetite destabilizes at T < 200°C to form maghemite (γ-Fe_2O_3) and H_2, which were detected by using a diversity of complementary analytical tools: Gas chromatography, X-ray diffraction, Mössbauer spectroscopy, and scanning electron microscopy. Our experiments demonstrate that the generation of H_2 from magnetite alteration by anoxic water is thermodynamically and kinetically favourable, as it formed at low temperature in a few weeks. In addition, numerical modeling attempting to reproduce those experiments failed to predict significant magnetite destabilization, Fe oxidation, and H_2 generation. To our mind, these results strongly suggest a lack of well constrained thermodynamic data in the literature concerning metastable Fe-oxides such as maghemite. Those values should be re-evaluated or reacquired to allow proper modeling and extrapolation over geological time scales. Nevertheless, major implications can be drawn from this work for natural environments. Regarding the genesis of BIF-hosted iron ores, the enrichment and oxidation of iron in BIF by groundwater leaching has long been a matter of interest and discussion. If secondary maghemite originating from primary magnetite destabilization is frequently observed in BIF alteration profiles, the mechanisms leading to such conversion remain unclear. Hence, this work could provide important clues in understanding part of the process of leaching-related Fe enrichment and oxidation in BIF. As for the future of native H_2 exploration, these results demonstrate that magnetite-rich lithologies should be targeted while exploring natural hydrogen resources. Furthermore, they show that H_2 generation in the subsurface at near-ambient temperature is possible, inferring that some H_2 emissions observed in cratonic areas could be of contemporaneous origin.

Data availability statement

The original contributions presented in the study are included in the article/Supplementary Material, further inquiries can be directed to the corresponding author.

Author contributions

UG, OS, IMa, and IMo produced the methodology. UG and VC conducted the experiments and participated in the subsequent analyses. MD performed the Mössbauer analyses. UG and TB realized the thermodynamic calculations. UG, TB, VC, and OS contributed to the final interpretations. UG wrote the manuscript and all authors contributed to its revision.

Funding

This work is part of the PhD project of UG, funded by MERSI and INSU-CNRS (TelluS).

Acknowledgments

The authors warmly thank Sophie Nowak (UPC) for XRD acquisitions and discussion, Stephan Borensztajn (IPGP) for the SEM sessions, François Guyot (IMPMC) for the always-illuminating conversations, Dan Levy (IPGP) for long talks and a careful review of the paper, Sonia Noirez (IFPen) for sharing her knowledge on gas chromatography, and Herman Ravelojaona (IFPen) for Rock-Eval analyses.

Conflict of interest

The authors declare that the research was conducted in the absence of any commercial or financial relationships that could be construed as a potential conflict of interest.

Publisher's note

Supplementary material

The Supplementary Material for this article can be found online at: https://www.frontiersin.org/articles/10.3389/feart.2023.1169356/full#supplementary-material

References

Allen, D. E., and Seyfried, W. E. (2004). Serpentinization and heat generation: Constraints from lost city and rainbow hydrothermal systems 1 1Associate editor: J. C. Alt. *Geochim. Cosmochim. Acta* 68, 1347–1354. doi:10.1016/j.gca.2003.09.003

Angerer, T., Duuring, P., Hagemann, S. G., Thorne, W., and McCuaig, T. C. (2015). A mineral system approach to iron ore in Archaean and Palaeoproterozoic BIF of Western Australia. *Geol. Soc. Lond. Spec. Publ.* 393, 81–115. doi:10.1144/SP393.11

Barbier, E. (2002). Geothermal energy technology and current status: An overview. *Renew. Sustain. Energy Rev.* 6, 3–65. doi:10.1016/S1364-0321(02)00002-3

Boreham, C. J., Edwards, D. S., Czado, K., Rollet, N., Wang, L., van der Wielen, S., et al. (2021a). Hydrogen in Australian natural gas: Occurrences, sources and resources. *APPEA J.* 61, 163. doi:10.1071/AJ20044

Boreham, C. J., Sohn, J. H., Cox, N., Williams, J., Hong, Z., and Kendrick, M. A. (2021b). Hydrogen and hydrocarbons associated with the neoarchean frog's leg gold camp, Yilgarn craton, western Australia. *Chem. Geol.* 575, 120098. doi:10.1016/j.chemgeo.2021.120098

Cannat, M. (1993). Emplacement of mantle rocks in the seafloor at mid-ocean ridges. *J. Geophys. Res. Solid Earth* 98, 4163–4172. doi:10.1029/92JB02221

Cornell, R. M., and Schwertmann, U. (2003). *The iron oxides: Structure, properties, reactions, occurrences and uses. 2., compl. Rev. And extended ed., repr*. Weinheim: Wiley VCH.

Crouzet, C., Brunet, F., Recham, N., Findling, N., Lanson, M., Guyot, F., et al. (2017). Hydrogen production by hydrothermal oxidation of FeO under acidic conditions. *Int. J. Hydrog. Energy* 42, 795–806. doi:10.1016/j.ijhydene.2016.10.019

Daniels, J. M., and Rosencwaig, A. (1969). Mössbauer spectroscopy of stoichiometric and non-stoichiometric magnetite. *J. Phys. Chem. Solids* 30, 1561–1571. doi:10.1016/0022-3697(69)90217-0

Duuring, P., Hagemann, S. G., Laukamp, C., and Chiarelli, L. (2019). Supergene modification of magnetite and hematite shear zones in banded iron-formation at Mt Richardson, Yilgarn Craton, Western Australia. *Ore Geol. Rev.* 111, 102995. doi:10.1016/j.oregeorev.2019.102995

Elder, T. (1965). Particle-size effect in oxidation of natural magnetite. *J. Appl. Phys.* 36, 1012–1013. doi:10.1063/1.1714076

Etiope, G. (2017). Abiotic methane in continental serpentinization sites: An overview. *Procedia Earth Planet. Sci.* 17, 9–12. doi:10.1016/j.proeps.2016.12.006

Etiope, G., Samardžić, N., Grassa, F., Hrvatović, H., Miošić, N., and Skopljak, F. (2017). Methane and hydrogen in hyperalkaline groundwaters of the serpentinized Dinaride ophiolite belt, Bosnia and Herzegovina. *Appl. Geochem.* 84, 286–296. doi:10.1016/j.apgeochem.2017.07.006

Frery, E., Langhi, L., Maison, M., and Moretti, I. (2021). Natural hydrogen seeps identified in the north perth basin, western Australia. *Int. J. Hydrog. Energy* 46, 31158–31173. doi:10.1016/j.ijhydene.2021.07.023

Gaucher, E. C. (2020). New perspectives in the industrial exploration for native hydrogen. *Elements* 16, 8–9. doi:10.2138/gselements.16.1.8

Geymond, U., Ramanaidou, E., Lévy, D., Ouaya, A., and Moretti, I. (2022). Can weathering of banded iron formations generate natural hydrogen? Evidence from Australia, Brazil and South Africa. *Minerals* 12, 163. doi:10.3390/min12020163

Grau-Crespo, R., Al-Baitai, A. Y., Saadoune, I., and De Leeuw, N. H. (2010). Vacancy ordering and electronic structure of γ - Fe $_2$ O $_3$ (maghemite): A theoretical investigation. *J. Phys. Condens. Matter* 22, 255401. doi:10.1088/0953-8984/22/25/255401

Hanesch, M. (2009). Raman spectroscopy of iron oxides and (oxy)hydroxides at low laser power and possible applications in environmental magnetic studies. *Geophys. J. Int.* 177, 941–948. doi:10.1111/j.1365-246X.2009.04122.x

Horsfield, B., Mahlstedt, N., Weniger, P., Misch, D., Vranjes-Wessely, S., Han, S., et al. (2022). Molecular hydrogen from organic sources in the deep Songliao Basin, P.R. China. *Int. J. Hydrog. Energy* 47, 16750–16774. doi:10.1016/j.ijhydene.2022.02.208

Joos, A., Rümenapp, C., Wagner, F. E., and Gleich, B. (2016). Characterisation of iron oxide nanoparticles by Mössbauer spectroscopy at ambient temperature. *J. Magn. Magn. Mater.* 399, 123–129. doi:10.1016/j.jmmm.2015.09.060

Klein, C. (2005). Some Precambrian banded iron-formations (BIFs) from around the world: Their age, geologic setting, mineralogy, metamorphism, geochemistry, and origins. *Am. Mineral.* 90, 1473–1499. doi:10.2138/am.2005.1871

Klein, F., Bach, W., and McCollom, T. M. (2013). Compositional controls on hydrogen generation during serpentinization of ultramafic rocks. *Lithos* 178, 55–69. doi:10.1016/j.lithos.2013.03.008

Klein, F., Tarnas, J. D., and Bach, W. (2020). Abiotic sources of molecular hydrogen on Earth. *Elements* 16, 19–24. doi:10.2138/gselements.16.1.19

Kuzmann, E., Nagy, S., and Vértes, A. (2003). Critical review of analytical applications of mössbauer spectroscopy illustrated by mineralogical and geological examples: (IUPAC technical report). *Int. Union Pure Appl. Chem.* 75, 801–858. doi:10.1515/iupac.75.0025

Larin, N., Zgonnik, V., Rodina, S., Deville, E., Prinzhofer, A., and Larin, V. N. (2015). Natural molecular hydrogen seepage associated with surficial, rounded depressions on the European craton in Russia. *Nat. Resour. Res.* 24, 369–383. doi:10.1007/s11053-014-9257-5

Lefeuvre, N., Truche, L., Donzé, F., Ducoux, M., Barré, G., Fakoury, R., et al. (2021). Native H $_2$ exploration in the western pyrenean foothills. *Geochem. Geophys. Geosystems* 22. doi:10.1029/2021GC009917

Malvoisin, B., and Brunet, F. (2023). Barren ground depressions, natural H2 and orogenic gold deposits: Spatial link and geochemical model. *Sci. Total Environ.* 856, 158969. doi:10.1016/j.scitotenv.2022.158969

Malvoisin, B., Brunet, F., Carlut, J., Rouméjon, S., and Cannat, M. (2012). Serpentinization of oceanic peridotites: 2. Kinetics and processes of san carlos olivine hydrothermal alteration: Kinetics of serpentinization. *J. Geophys. Res. Solid Earth* 117. n/a-n/a. doi:10.1029/2011jb008842

Mayhew, L. E., Ellison, E. T., McCollom, T. M., Trainor, T. P., and Templeton, A. S. (2013). Hydrogen generation from low-temperature water–rock reactions. *Nat. Geosci.* 6, 478–484. doi:10.1038/ngeo1825

McCollom, T. M. (2016). Abiotic methane formation during experimental serpentinization of olivine. *Proc. Natl. Acad. Sci.* 113, 13965–13970. doi:10.1073/pnas.1611843113

McCollom, T. M., and Bach, W. (2009). Thermodynamic constraints on hydrogen generation during serpentinization of ultramafic rocks. *Geochim. Cosmochim. Acta* 73, 856–875. doi:10.1016/j.gca.2008.10.032

Milesi, V., Guyot, F., Brunet, F., Richard, L., Recham, N., Benedetti, M., et al. (2015). Formation of CO2, H2 and condensed carbon from siderite dissolution in the 200–300°C range and at 50MPa. *Geochim. Cosmochim. Acta* 154, 201–211. doi:10.1016/j.gca.2015.01.015

Moretti, I., Brouilly, E., Loiseau, K., Prinzhofer, A., and Deville, E. (2021). Hydrogen emanations in intracratonic areas: New guide lines for early exploration basin screening. *Geosciences* 11, 145. doi:10.3390/geosciences11030145

Moretti, I., Geymond, U., Pasquet, G., Aimar, L., and Rabaute, A. (2022). Natural hydrogen emanations in Namibia: Field acquisition and vegetation indexes from multispectral satellite image analysis. *Int. J. Hydrog. Energy* 47, 35588–35607. doi:10.1016/j.ijhydene.2022.08.135

Morris, R. C., and Ramanaidou, E. R. (2007). Genesis of the channel iron deposits (CID) of the Pilbara region, Western Australia. *Aust. J. Earth Sci.* 54, 733–756. doi:10.1080/08120090701305251

Nazarova, K. A. (1994). Serpentinized peridotites as a possible source for oceanic magnetic anomalies. *Mar. Geophys. Res.* 16, 455–462. doi:10.1007/BF01270519

Nazarova, K. A., Wasilewski, P. J., and Dick, H. J. B. (2000). Magnetic study of serpentinized harzburgites from the islas orcadas fracture zone. *Mar. Geophys. Res.* 21, 475–488. doi:10.1023/A:1026550011802

Neubeck, A., Duc, N. T., Bastviken, D., Crill, P., and Holm, N. G. (2011). Formation of H2 and CH4by weathering of olivine at temperatures between 30 and 70°C. *Geochem. Trans.* 12, 6. doi:10.1186/1467-4866-12-6

Potter, J., Salvi, S., and Longstaffe, F. J. (2013). Abiogenic hydrocarbon isotopic signatures in granitic rocks: Identifying pathways of formation. *Lithos* 182–183, 114–124. doi:10.1016/j.lithos.2013.10.001

Prinzhofer, A., Cissé, C. S. T., and Diallo, A. B. (2018). Discovery of a large accumulation of natural hydrogen in Bourakebougou (Mali). *Int. J. Hydrog. Energy* 43, 19315–19326. doi:10.1016/j.ijhydene.2018.08.193

Ramanaidou, E. R., and Wells, M. A. (2014). "Sedimentary hosted iron ores," in *Treatise on Geochemistry* (Elsevier), 313–355. doi:10.1016/B978-0-08-095975-7.01115-3

Saad, A. H. (1969). Magnetic properties of ultramafic rocks from Red Mountain, California. *GEOPHYSICS* 34, 974–987. doi:10.1190/1.1440067

Salvi, S., and Williams-Jones, A. E. (1997). Fischer-Tropsch synthesis of hydrocarbons during sub-solidus alteration of the Strange Lake peralkaline granite, Quebec/Labrador, Canada. *Geochim. Cosmochim. Acta* 61, 83–99. doi:10.1016/S0016-7037(96)00313-4

Swaddle, T. W., and Oltmann, P. (1980). Kinetics of the magnetite–maghemite–hematite transformation, with special reference to hydrothermal systems. *Can. J. Chem.* 58, 1763–1772. doi:10.1139/v80-279

Truche, L., Bourdelle, F., Salvi, S., Lefeuvre, N., Zug, A., and Lloret, E. (2021). Hydrogen generation during hydrothermal alteration of peralkaline granite. *Geochim. Cosmochim. Acta* 308, 42–59. doi:10.1016/j.gca.2021.05.048

Tutolo, B. M., Seyfried, W. E., and Tosca, N. J. (2020). A seawater throttle on H $_2$ production in Precambrian serpentinizing systems. *Proc. Natl. Acad. Sci.* 117, 14756–14763. doi:10.1073/pnas.1921042117

Vacquand, C., Deville, E., Beaumont, V., Guyot, F., Sissmann, O., Pillot, D., et al. (2018). Reduced gas seepages in ophiolitic complexes: Evidences for multiple origins of the H2-CH4-N2 gas mixtures. *Geochim. Cosmochim. Acta* 223, 437–461. doi:10.1016/j.gca.2017.12.018

Winsett, J., Moilanen, A., Paudel, K., Kamali, S., Ding, K., Cribb, W., et al. (2019). Quantitative determination of magnetite and maghemite in iron oxide nanoparticles using Mössbauer spectroscopy. *SN Appl. Sci.* 1, 1636. doi:10.1007/s42452-019-1699-2